Structure of ^{14}C via elastic and inelastic neutron scattering from ^{13}C: Measurement and R-matrix analysis

D. A. Resler,* H. D. Knox, P. E. Koehler,† and R. O. Lane
Ohio University, Athens, Ohio 45701

G. F. Auchampaugh
Los Alamos National Laboratory, Los Alamos, New Mexico 87545

(Received 27 May 1988)

Differential cross sections for neutrons elastically scattered from ^{13}C and inelastically scattered to the first three excited states $^{13}C^*$(3.09, 3.68, and 3.85 MeV) were measured at 69 incident energies for $4.5 \leq E_n \leq 11$ MeV. A multiple scattering code provided a simulation of the experimental scattering process allowing accurate corrections to the small measured inelastic cross sections. The integrated $^{13}C(n,\alpha)^{10}Be$ cross section was determined by subtracting the sum of the measured integrated cross sections from the total. Shell-model calculations were used to generate the R-matrix parameters for the elastic and first three inelastic channels of $^{13}C+n$, and, after some minor adjustments, the predicted structure generally agreed with experiment for $E_n < 4$ MeV. Previous elastic $^{13}C+n$ data were refitted to replace constant R_0 R-matrix background terms by more realistic broad states and to achieve better agreement with model calculations and the data. R-matrix fitting of the full data set produced new ^{14}C level information. For $E_n > 4$ MeV ($E_x > 12$ MeV), five states were given definite J^π assignments and three states tentative assignments.

I. INTRODUCTION

Previous to this work, no states had been given definite spin or parity assignments[1,2] above an excitation energy of $E_x \approx 12.4$ MeV in ^{14}C. Direct reactions such as $^9Be(^6Li,p)^{14}C$ Ref. 3, $^{12}C(t,p)^{14}C$ Refs. 4 and 5, $^{13}C(d,p)^{14}C$ Ref. 6, and others[7–16] had revealed narrow states in ^{14}C above an excitation energy of $E_x = 12.4$ MeV, however, even when it was possible to make assignments of spin and parity, they were either tentative or conflicting.

Early neutron total cross section measurements for $^{13}C+n$ by Cohn *et al.*[17] showed obvious resonance structure. The more recent high resolution neutron total cross section measurements of Auchampaugh *et al.*[18] yielded much more detail of narrow and broad resonances up to a neutron energy of $E_n = 14$ MeV ($E_x \approx 21$ MeV). A series of elastic neutron scattering measurements for $^{13}C+n$ were carried out at the Ohio University John E. Edwards Accelerator Laboratory (OUAL) previous to the present work for neutron energies of $1.25 \leq E_n \leq 6.5$ MeV ($9.3 \leq E_x \leq 14.2$ MeV) by Lane *et al.*[2] These data displayed very definite resonance behavior. The R-matrix analysis[2] of the combined broad structure observed in Ref. 2 together with the narrow resonances observed in Ref. 18 was very successful in making spin and parity assignments for new levels in ^{14}C.

The success of these elastic scattering measurements and subsequent R-matrix analysis indicated the study should be extended to higher energies. For the present work measurements of the differential cross sections for neutrons elastically scattered from ^{13}C and inelastically scattered to the first three excited states $^{13}C^*$ (3.09, 3.68, and 3.85 MeV) were made for incident neutron energies of $4.55 \leq E_n \leq 11$ MeV ($12.4 \leq E_x \leq 18.4$ MeV). A discussion of the experimental procedures and results are given in the next section and the R-matrix analysis of the $^{13}C+n$ data in the following section.

II. EXPERIMENTAL PROCEDURE AND RESULTS

A. Experimental procedure

1. Facilities

The measurements of neutron differential elastic and inelastic cross sections for this work were carried out in seven separate experiments from December 1978 to February 1983 at the OUAL.[19–21] Standard time-of-flight (TOF) techniques were used for all the measurements, but the methods were varied from one experiment to the next because many improvements were made to the facilities and techniques used over the time period of these measurements. The most notable improvement was the construction of the Beam Swinger Facility during the Fall of 1980.[22] A brief description of the experimental procedure follows with specific details available in Ref. 23 and references therein.

For all but one of the measurements, beams of protons, pulsed and bunched to subnanosecond widths at repetition rates of 5 or 2.5 MHz and with average currents of 2–4 μA, were incident upon a 3.3-cm long gas cell containing approximately 1.6 atm of tritium gas. Monoenergetic neutrons were thereby produced through the $^3H(p,n)^3He$ reaction. For the remaining experiment, deuteron beams were incident upon a gas cell of deuterium and monoenergetic neutrons were produced through the $^2H(d,n)^3He$ reaction.

The scattering sample consisted of 40.75 g of very fine ^{13}C powder packed into a thin-walled aluminum can of

mass 8.08 g. The carbon was enriched to 98.0-atom-percent ^{13}C (2.0-atom-percent ^{12}C). Multiple scattering analyses of the data[24,23] showed a 2.2-atom-percent impurity of hydrogen, presumably in the form of water. The sample-in can had an inside diameter of 3.6 cm and a height of 3.2 cm. An identical empty aluminum can was used for sample-out measurements.

Depending on the measurement, the main detector system employed either a flat or dynamic bias[22] and consisted of either a single NE 213 scintillator (5 cm thick by 11.25 cm diameter or 10 cm thick by 20 cm diameter) or an array of three NE 213 scintillators (each 5 cm thick by 11.25 cm diameter) each optically coupled to an RCA 4522 or RCA 8854 photomultiplier tube using a plastic light guide. Flight paths ranged from 15 to 20 cm for the source-to-sample distance, 2.3 to 6.3 m for the sample-to-detector distance, and 0.8 to 4.9 m for the source-to-monitor distance.

2. Data reduction

The conversion of counts to cross section is described elsewhere.[23] Corrections were made for air scattering (factors of 0.95 to 1.15 depending on the experiment), flux attenuation and source anisotropy (factors of ≈ 1.15), and multiple scattering. In order to accurately calculate the multiple scattering corrections, a new code MACHO was developed.[24,23] Because of the accurate simulation of the neutron scattering process, it was possible to make reliable corrections for the following difficulties encountered in the present work: (1) the small inelastic cross sections appeared on top of elastic scattering of the source continuum; (2) the scattering from a 2.2-atom-percent impurity of hydrogen often fell under the small inelastic cross sections; and (3) the inelastic scattering to the second and third excited states was not well resolved. Correction factors typically ranged from 0.85 to 1.20. The errors on these correction factors were comparable to the counting-statistics errors in the original data.

A conservative error of 1% was assigned to quantities which depend on flight paths and the number of nuclei in the sample. Errors due to counting statistics were typically 1% or less for the elastic data, and for the inelastic data, errors were typically 3 to 6%. There was a 3% error assigned to the measurement of the detector's relative efficiency and the shape of the source neutron cross section is known to 1%. Combining all the possible sources of error it was determined that the elastic data were measured to within 5% and the inelastic data to within 5–15 %.

B. Experimental results

The final experimental results for this work are presented in this section. Neutron elastic and inelastic differential scattering cross section measurements were also made concurrently for ^{11}B+n Ref. 25, ^{6}Li+n Ref. 26, and ^{18}O+n Ref 27. As an additional check on our system, measurements of well-established ^{12}C+n differential scattering cross sections agreed with previous data within quoted errors.[23]

1. Present work

Measurements of ^{13}C+n elastic and inelastic differential cross sections were made at 69 incident energies from $E_n = 4.55$ MeV to $E_n = 10.99$ MeV. Elastic scattering cross sections were measured at all energies as were inelastic scattering cross sections to the first excited state ($Q = -3.09$ MeV). Inelastic scattering cross sections to the second excited state ($Q = -3.68$ MeV) and to the third excited state ($Q = -3.85$ MeV) were measured at all energies above $E_n = 5.5$ MeV (60 energies). Angular distributions were measured in the laboratory system from 15° to 160° at 9 to 11 angles. In all, 2742 differential cross sections for ^{13}C+n were measured. Examples of subtracted TOF spectra can be found in Refs. 23 and 24.

Representative angular distributions are displayed for all four measured groups in Figs. 1, 2, 3, and 4. The lines through the points are the results of least-squares fitting the data with a series of Legendre polynomials, $\sigma(\theta) = \sum B_L P_L(\cos\theta)$. As shown in the figures, the angular distributions, and hence the B_L, change dramatically in shape and magnitude as a function of incident neutron energy. Plots of the B_L coefficients are shown for all four measured groups in Figs. 5, 6, 7, and 8. All of the data displayed below $E_n = 7.5$ MeV were taken with an incident energy spread of about 80 keV, whereas, all the data displayed above $E_n = 7.5$ MeV were taken with an incident energy spread of about 120 keV. The high resolution total cross section data of Auchampaugh *et al.*[18] showed very narrow resonances near $E_n \approx 5.1$ MeV and $E_n \approx 7.2$ MeV and because of our larger resolution we excluded angular distributions near these energies.

Only coefficients through B_6 were required to fit the elastic scattering data. For the inelastic data, only coefficients through B_4 were required to fit the data below $E_n = 7.5$ MeV. Above $E_n = 7.5$ MeV, coefficients through B_6 are shown for the inelastic data but B_6 still appears to be statistically zero. Implications of this on the structure of states in the compound nucleus ^{14}C will be discussed in a later section.

2. Comparisons with other data

A literature search has revealed only three other experimental studies of ^{13}C+n elastic differential scattering.[2,28,29] Two of these studies[2,29] were done at Ohio University using the same sample as this work. Petler *et al.*[29] measured the differential elastic scattering cross section for ^{13}C+n at $E_n = 24$ MeV—too high an energy for comparison with the present work. Lane *et al.*[2] measured the elastic scattering differential cross sections for ^{13}C+n for $1.25 \leq E_n \leq 6.5$ MeV. Over the 2 MeV region of overlap, the agreement is excellent (Fig. 5). In the other remaining study, Davè *et al.*[28] measured elastic scattering differential cross sections for ^{13}C+n at $E_n = 10$, 12, 14, 16, and 18 MeV. As can be seen in Fig. 5, the agreement is very good between the measurements of the present work and those of Davè *et al.*[28] at the only overlap energy ($E_n = 10$ MeV)—especially since at this energy there is a large valley in all the B_L values.

The only other $^{13}C+n$ inelastic scattering differential cross section measurements are also by Davè *et al.*[28] at $E_n = 10$ MeV. A comparison of the measurement for the inelastic scattering angular distribution to the first excited state is shown in Fig. 9. Since Davè *et al.*[28] were unable to resolve inelastic scattering to the second and third excited states, the resolved data of the present work has been added together for comparison of the measurements of the combined inelastic scattering angular distribution shown in Fig. 10. Although the agreement is good for the data to the first excited state, the agreement (especially in magnitude) for the combined second and third excited states is not as good.

On the basis of a comparison at a single energy, it is difficult to explain the differences between the two measurements. However, the inelastic B_L values undergo rapid changes around $E_n = 10$ MeV (see Figs. 7 and 8). A slight error in incident energy (or averaging over different energy spreads) might account for the differences in absolute magnitude. The accuracy to which the present measurements were made has been shown[23] through the ^{12}C checks and the consistency of the data at the overlap points.

The ratio of the zero-degree center-of-mass elastic cross section (estimated from the Legendre polynomial expansion) to Wick's limit[30] has been calculated.[23] According to Wick's theorem, this ratio should always be greater than or equal to unity. In all cases, except for three energies just above $E_n = 10$ MeV, this condition held true, with the other three values being just outside of the error estimates.

3. *Estimation of unmeasured cross sections*

For $E_n \leq 13.38$ MeV, the threshold for the charged-particle-producing reaction $^{13}C(n,t)^{11}B$, only the (n,n'), (n,α), and $(n,2n)$ particle-producing reactions are possible. Therefore, ignoring the very small capture cross section $^{13}C(n,\gamma)^{14}C$, the result of subtracting the sum of the integrated elastic cross section plus integrated inelastic cross sections to the first through third excited states from the total should be equal to the sum of the (n,α) and $(n,2n)$ cross sections because all higher inelastic scatterings would be to states unbound to neutron emission. The present work included a measurement of the $(n,2n)$ cross section at $E_n = 8.25$ MeV.[31] Preliminary $(n,2n)$ measurements of Cates and co-workers[32,33] are also discussed in Ref. 31. By subtracting the $(n,2n)$ results from the estimated sum of the (n,α) and $(n,2n)$ cross sections obtained as previously described, the (n,α)

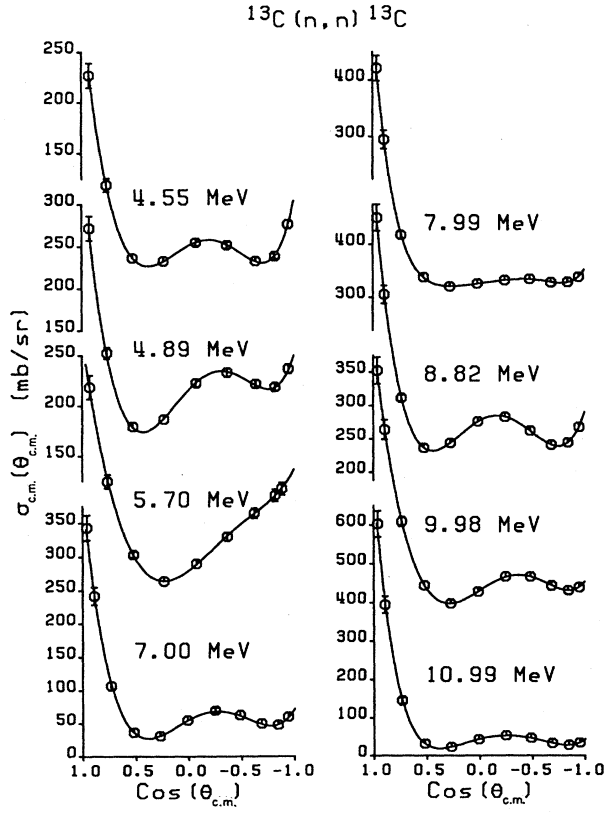

FIG. 1. Representative angular distributions for $^{13}C(n,n)^{13}C$ from the present work. The lines are Legendre polynomial fits to the data.

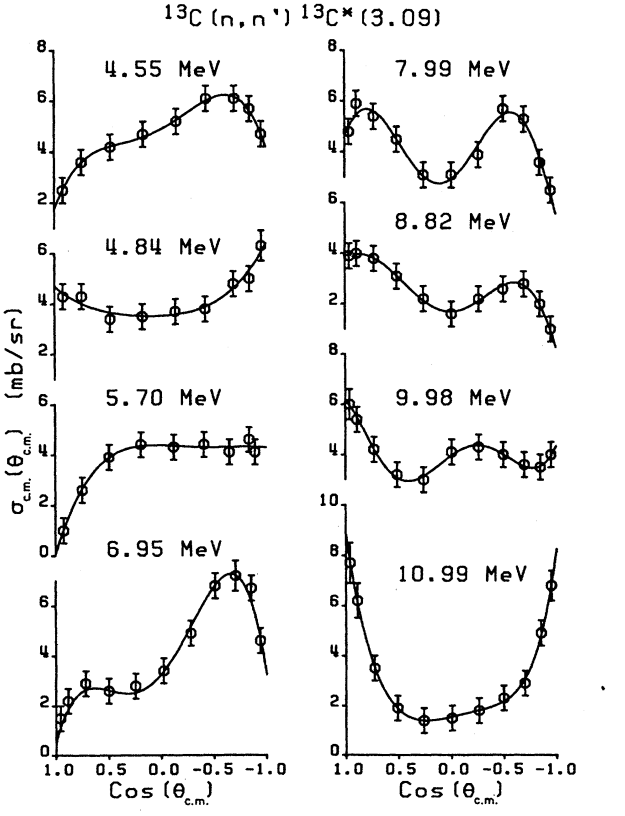

FIG. 2. Representative angular distributions for $^{13}C(n,n')^{13}C^*(3.09)$ from the present work. The lines are Legendre polynomial fits to the data.

integrated cross section can be estimated.

Estimations of the (n,α) integrated cross section are shown in Fig. 11. For $5.5 \leq E_n \leq 7.9$ MeV, an upper limit to the (n,α) integrated cross section was taken to be the estimated sum of the (n,α) and $(n,2n)$ integrated cross sections. From the work of Cates and coworkers,[32,33] it appears that the $(n2,n)$ integrated cross section is small below $E_n \approx 8$ MeV. For $7.9 \leq E_n \leq 11$ MeV, the (n,α) integrated cross section was obtained by subtracting the $(n,2n)$ integrated cross sections of the present work[31] and Cates and coworkers[32] from the estimated sum of the (n,α) and $(n,2n)$ integrated cross sections. Although the errors are large, this gives an experimental estimate of the (n,α) integrated cross section.

III. *R*-MATRIX ANALYSES

The experimental results for the present work display very definite resonance behavior throughout the entire energy range. This is indicative of the formation of strong compound nuclear states in ^{14}C up to $E_x \approx 20$ MeV. The *R*-matrix formalism of Lane and Thomas[34] was used to extract structure information on the compound nucleus ^{14}C from these data. Two approaches were taken. The first and more usual approach involves determining the *R*-matrix parameters by fitting the available data. Complications in this method can arise which limit its usefulness.[26,23] A second approach which ameliorates those complications involves the prediction of the initial set of *R*-matrix parameters by shell model calculations.[26,23]

For energies of this study, only the neutron and alpha particle channels are open. The separation energy for ^{10}Be$+\alpha$ occurs at $E_x(^{14}\text{C}) = 12.012$ MeV. Since the ^{13}C$(n,\alpha)^{10}$Be cross section has been shown to be small, it was not included in the current analyses. The particle channel, ^{11}B$+t$, opens at $E_x(^{14}\text{C}) = 20.598$ MeV—well above the region of current interest. Thus, only the ^{13}C$+n$ and ^{13}C$^*+n'$ reaction channels need be included. Eleven inelastic ^{13}C$^*+n'$ channels are possible at the highest energy measured, $E_x = 18.4$ MeV ($E_n = 11$ MeV). However, only the first three were included along with the elastic channel because the cross sections to the remaining excited states appear to be small[23] and detailed data for comparisons currently exist only for the elastic and first three inelastic ^{13}C$+n$ particle channels.

An examination of the data reveals that all of the angular distributions for $E_n < 11$ MeV are fitted by seven or fewer Legendre expansion coefficients. In most cases, the B_6 term is statistically zero or very close to zero. For the

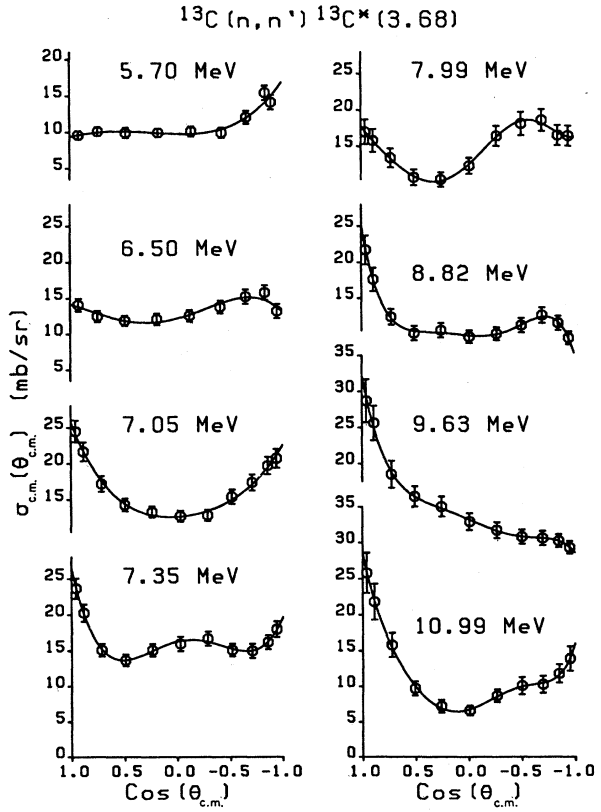

FIG. 3. Representative angular distributions for ^{13}C$(n,n')^{13}$C*(3.68) from the present work. The lines are Legendre polynomial fits to the data.

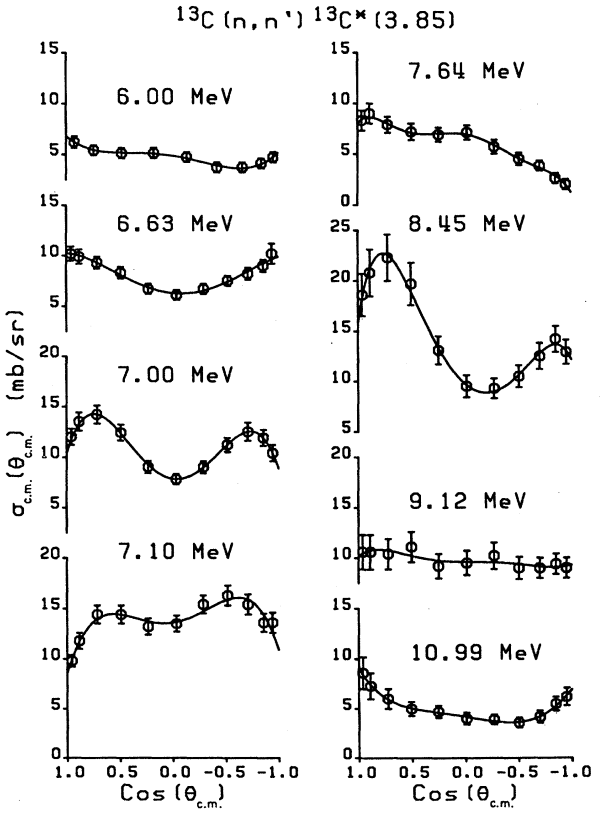

FIG. 4. Representative angular distributions for ^{13}C$(n,n')^{13}$C* (3.85) from the present work. The lines are Legendre polynomial fits to the data.

TABLE I. Boundary conditions corresponding to $E_n = 5.5$ MeV.

l value	Channel Elastic	1st	2nd	3rd
0	0.0	0.0	0.0	0.0
1	−0.18	−0.35	−0.44	−0.47
2	−0.72	−1.32	−1.51	−1.56
3	−1.85	−2.58	−2.71	−2.75

elastic data, the B_6 term is definitely nonzero at energies above $E_n \approx 7.5$ MeV, although it is small. Some resonance structure is observed in the elastic and inelastic data for the B_5 term. Thus, only partial waves up to $l=2$ are very important in the $^{13}C+n$ scattering processes for $E_n < 11$ MeV. However, the small presence of B_6 indicates that $l=3$ is required in some instances. Also, the structure observed in the B_5 term is most probably the result of $l=2$ resonances interfering with an $l=3$ background (since B_6 is small and B_4 is large). We therefore allowed up to $l=3$ for the elastic and three inelastic channels. For the elastic or entrance channel, nine J^π values are allowed: $0^\pm$, $1^\pm$, $2^\pm$, $3^\pm$, and 4^+. Decay by inelastic channels of up to $l=3$ would allow some higher J^π values; however, they are not included since they cannot be reached through the entrance channel for $l \leq 3$.

Final boundary conditions (Table I) were chosen to be equal to the channel shift factors corresponding to $E_n = 5.5$ MeV—half the value of the highest incident neutron energy of this work. When fitting by adjusting the parameters, this is the optimum choice of boundary conditions.[23] For the R-matrix parameters obtained from shell model predictions, the optimum choice of boundary conditions is different (see the next section) but they can be transformed to the above mentioned boundary conditions.[23] The channel radii were assumed to be the same for the elastic and three inelastic channels. A channel radius of 4.5 fm was used—the same as used in the $^{13}C+n$ work of Lane *et al.*[2]

A. Fits based on shell-model predictions

In this section, R-matrix fits based on shell-model predictions will be presented. Two different shell-model calculations were tried.[23] The first is from Resler[35] in which calculations for the normal and non-normal parity states of ^{13}C and ^{14}C were performed in the full $(0+1)\hbar\omega$ model space. The second is from Millener and Darema-Rogers[36,37] (MDR) who used the Cohen and Kurath[38] (8-16)POT interaction for the $1p$ shell matrix elements and the Millener and Kurath[39] particle-hole interaction for the $1p$-$2s1d$ matrix elements.

Single-nucleon spectroscopic amplitudes were obtained

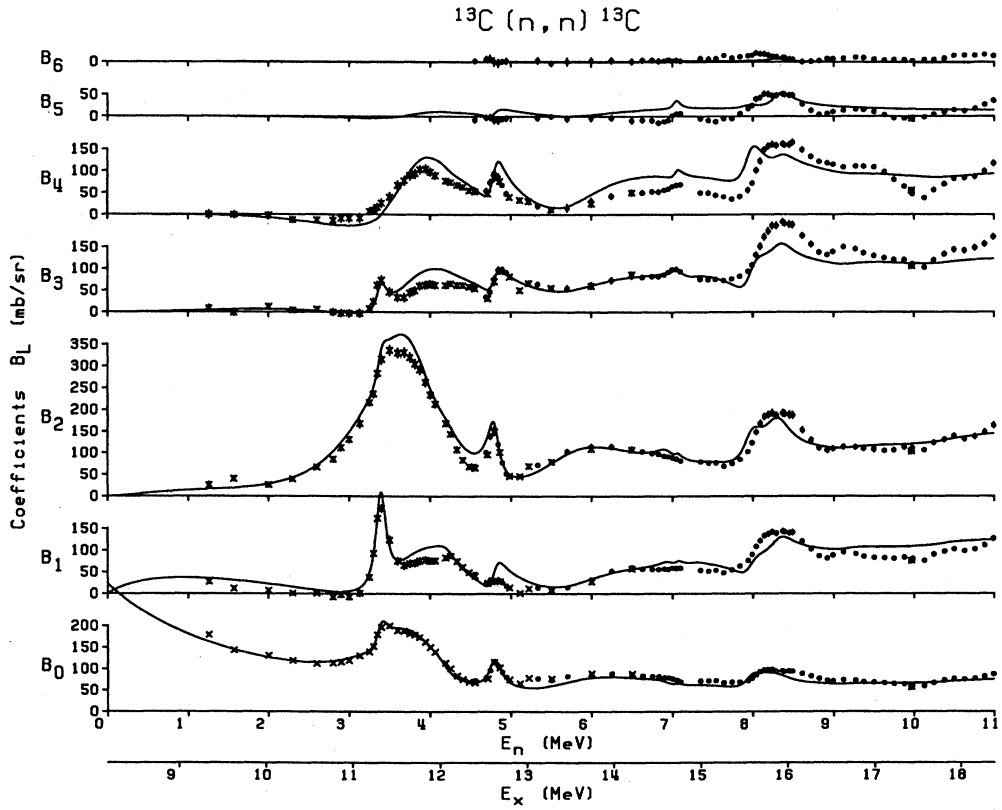

FIG. 5. Comparison of the best adjustment-of-parameters R-matrix fits to the elastic data of Lane *et al.* (Ref. 2) (×) ($0 \leq E_n \leq 6.5$ MeV), of the present work (●) ($4.55 \leq E_n \leq 11$ MeV), and of Davè *et al.* (Ref. 28) (*) ($E_n = 10$ MeV).

for $^{13}C+n \leftrightarrow {}^{14}C$. The shell-model quantities were then transformed to R-matrix input by the following. For channel c and level λ of a given J^{π}, the R-matrix reduced width amplitudes $\gamma_{\lambda c}$ were obtained from the shell-model spectroscopic amplitudes $S_{\lambda c}^{1/2}$ by the transformation

$$\gamma_{\lambda c}=\left[\frac{3\hbar^2}{2\mu_c a_c^2}\right]^{1/2}\theta_c^0 S_{\lambda c}^{1/2}\ , \tag{1}$$

where μ_c is the reduced channel mass, a_c is the channel radius, and θ_c^0 is the dimensionless single-particle reduced width amplitude which is defined by

$$\theta_c^0=(\tfrac{1}{3}r_0^3)^{1/2}R_l(r_0)\ , \tag{2}$$

where $R_l(r)$ is the radial wave function and r_0 is the radius for the nuclear surface (usually assumed to be equal to a_c).

In principle, θ_c^0 can be calculated from the shell-model wave functions, but in general this is not the best procedure.[40] While the shell-model wave functions can agree reasonably well with the real nuclear wave functions of the internal region as defined by the R matrix, these wave functions may be very different near the boundary or nuclear surface. Therefore, large errors could result from using shell-model wave functions to evaluate θ_c^0. Commonly, θ_c^0 is found empirically by comparing values of $\gamma_{\lambda c}/(3\hbar^2/2\mu_c a_c^2)^{1/2}$, determined by the R-matrix fitting of experimental data, with the calculated spectroscopic amplitudes $S_{\lambda c}^{1/2}$. Following Lane *et al.*,[2] the dimensionless single-particle reduced width amplitudes θ_c^0 were taken as the following: $\theta^0_{s_{1/2}}=0.42$, $\theta^0_{p_{1/2}}=\theta^0_{p_{3/2}}=0.50$, and $\theta^0_{d_{3/2}}=\theta^0_{d_{5/2}}=0.63$.

The transformation between R-matrix level energies E_λ and the shell-model excitation energies E_{x_λ} almost always involves what is known as the single-level approximation:

$$E_\lambda=E_{\text{c.m.}_\lambda}+\sum_c (S_c-B_c)\gamma_{\lambda c}^2\ , \tag{3}$$

where the center-of-mass energy $E_{\text{c.m.}_\lambda}$ is given by $E_{x_\lambda}-E_{\text{sep}}$ and E_{sep} is the channel separation energy. The shift factor S_c is evaluated for each channel at the center-of-mass energy $E_{\text{c.m.}_\lambda}$.

In using the adjustment-of-parameters method of R-matrix fitting, the boundary conditions B_c are dependent only on the pair of particles (channel) and l value with

$$B_c=S_c(E_{\text{middle}})\ , \tag{4}$$

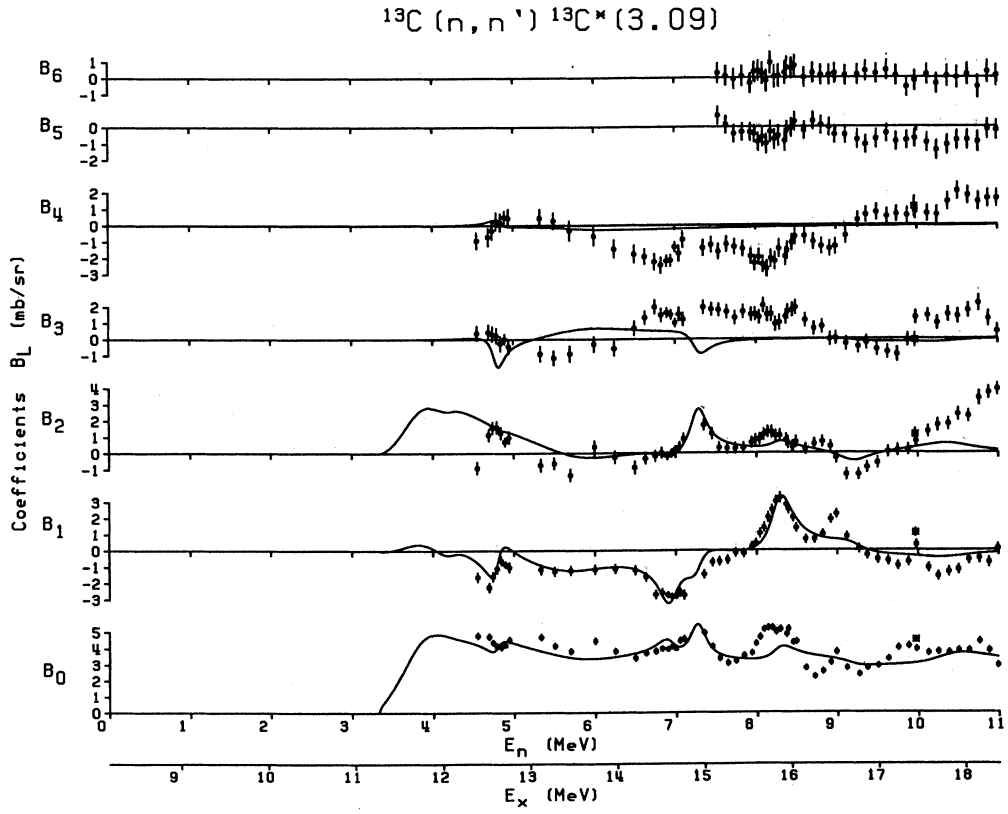

FIG. 6. Comparison of the best adjustment-of-parameters R-matrix fits to the $^{13}C(n,n')^{13}C^*$ (3.09) data of the present work (●) ($4.55 \le E_n \le 11$ MeV), and of Davè *et al.* (Ref. 28) (*) ($E_n = 10$ MeV).

where E_{middle} is the center-of-mass energy which corresponds to approximately the middle of the region being studied. This choice of boundary conditions produces, on the average, the minimum shift between level energies and the corresponding excitation energies. When doing only fitting of parameters, this is the best choice that can be made for the boundary conditions.

However, when predicting the R-matrix parameters from shell-model calculations, a different initial set of boundary conditions is better. According to Barker[41–45] the optimal set of boundary conditions is determined by the nature of the shell-model calculations. In the case of a single isolated level,[34] the boundary conditions B_c should be chosen so that the level energy E_λ lies within the width of the observed resonance for the one-level approximation to be most accurate. Thus, the boundary conditions $B_c \approx S_c$ produce the best results. For the multilevel case, Barker's prescriptions have the result of optimizing the use of the single-level approximation for each level to which it is applied.

The extreme choice of boundary conditions is to choose a different B_c for each level λ,[41,44,45]

$$B_{c_\lambda} = S_c(E_{\text{c.m.}_\lambda}) \ . \tag{5}$$

This is appropriate when the shell-model states of different configurations are involved. However, in an R-matrix calculation, a single set of boundary conditions B_c' is used for all levels of a given J^π. Therefore, the R-matrix parameters obtained using the boundary conditions B_{c_λ} must be transformed to a set B_c'. Such a transformation is usually not obvious. Except for the simple cases involving relatively few levels,[44,45] this method must be abandoned.

It has been suggested by Barker[41–43] that the best agreement between the R-matrix eigenstates and the shell-model wave functions on the one hand, and the internal part of the actual wave function on the other, is expected with

$$B_c = S_c(\bar{E}_{\text{c.m.}}) \ , \tag{6}$$

where $\bar{E}_{\text{c.m.}}$ is a mean energy weighted in some manner by the level strengths and therefore independent of level λ but possibly dependent on c and J^π. This choice of boundary conditions is best when the shell-model states are of the same configuration. The mean energy $\bar{E}_{\text{c.m.}}$ can be found from

$$\bar{E}_{\text{c.m.}} = \frac{\sum_\lambda (\gamma_{\lambda c}^2)^p E_{\text{c.m.}_\lambda}}{\sum_\lambda (\gamma_{\lambda c}^2)^p} \ , \tag{7}$$

for some value of p.[42] There are three obvious choices

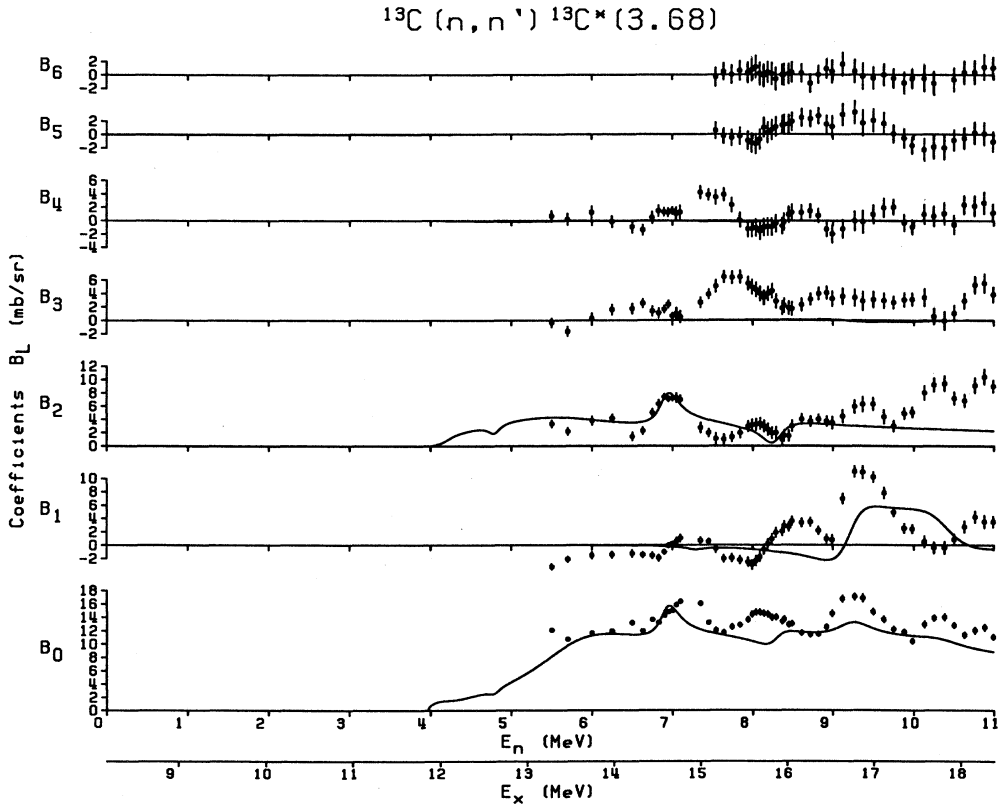

FIG. 7. Comparison of the best adjustment-of-parameters R-matrix fits to the $^{13}C(n,n')^{13}C^*$ (3.68) data of the present work.

for some value of p.[42] There are three obvious choices for p: $p=1$, $p\rightarrow\infty$, or p somewhere in between. Following Barker's suggestion,[41] Knox *et al.*[26] chose $p\rightarrow\infty$ for their work on the lithium isotopes. With that choice, $\bar{E}_{\text{c.m.}}$ is given by the energy of the state λ with the largest reduced width $\gamma^2_{\lambda c}$ as predicted by the shell model. Furthermore, Knox *et al.* assumed $E_\lambda = E_{\text{c.m.}}$ [as compared with Eq. (3)].

We earlier mentioned that the best choice of boundary conditions optimized the use of the single-level approximation when applied individually to each level of a multilevel problem. In other words, the best choice of boundary conditions minimizes the difference between the level energies and the center-of-mass energies. An investigation has been made in the present work[23] for minimizing

$$\sum_\lambda (E_{\text{c.m.}_\lambda} - E_\lambda)^2 , \tag{8a}$$

or equivalently,

$$\sum_\lambda \left[\sum_c (S_c - B_c)\gamma^2_{\lambda c} \right]^2 , \tag{8b}$$

by varying p in Eq. (7) such that p was independent of J^π. Those results show that the function (8) is slowly varying with changing p, with the minimum occurring for $3 < p < 6$—the specific value of p depending on the shell-model calculation used. Also, $p\rightarrow\infty$ was found to be somewhat better than $p=1$. For the choice $p\rightarrow\infty$, the function (8a) is about as small as it can be made and the assumption $E_\lambda = E_{\text{c.m.}_\lambda}$ made by Knox *et al.*[26] is probably reasonable. Many times, most of the total strength for a given angular momentum channel occurs in a single state. This easily explains the very shallow dependence of the rms deviation with p. In the extreme case of all the strength occurring in a single state for any of the angular momentum channels, the rms deviation would be independent of p.

Using a value of $p=4$, R-matrix calculations were made from the shell-model calculations of Resler[35] and of MDR.[36,37] Shown in Fig. 12 are the results for the elastic scattering group as obtained from the R-matrix parameters of Table II based on Resler's calculations, and in Fig. 13, for parameters based on MDR's calculations. The first apparent problem is that both calculations are much higher than the data for all the coefficients. This is caused by a major shortcoming of the model calculations: i.e., the omission of normal parity states arising from the more complicated (and hence more difficult to calculate) $2\hbar\omega$ and higher configurations. In the calculation of Resler, only the five $0\hbar\omega$ $1p$ shell normal parity states were included and for MDR no normal parity states were included. However, the R-matrix formalism contains functions arising from the boundary conditions that contribute to the scattering by all orders of partial waves,

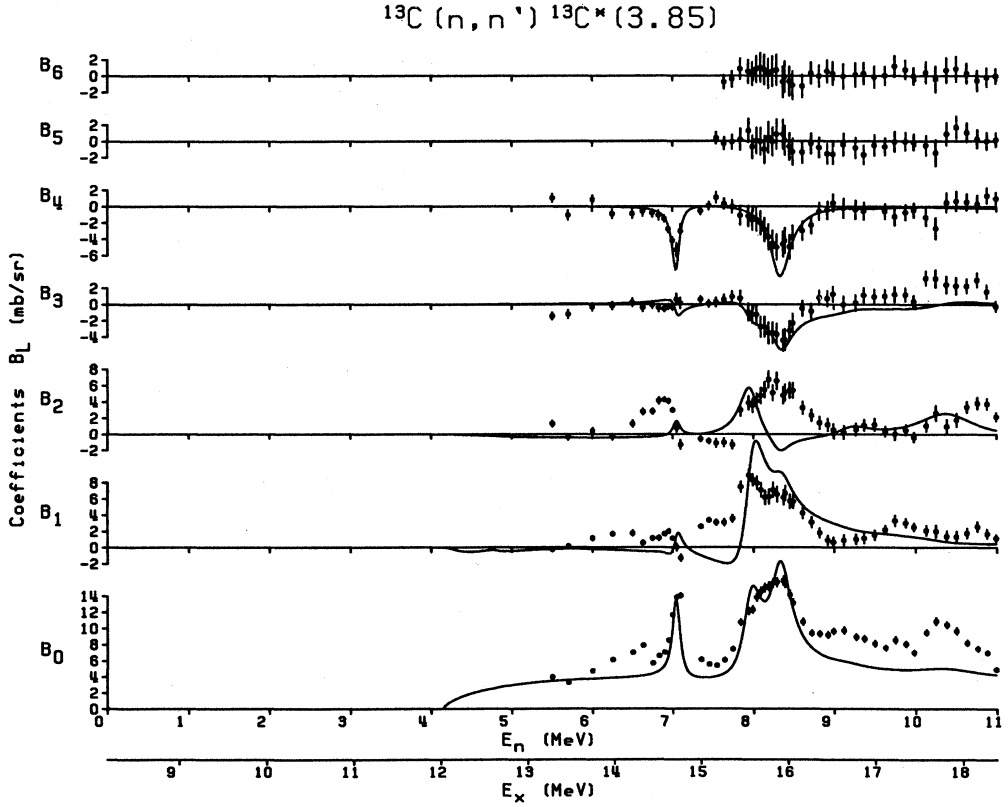

FIG. 8. Comparison of the best adjustment-of-parameters R-matrix fits to the ^{13}C$(n,n')^{13}$C* (3.85) data of the present work.

TABLE II. *R*-matrix parameters predicted by the shell-model calculations of Resler (Ref. 35).

J^π	E_λ (MeV)	$\gamma_{\lambda c}$ ($MeV^{1/2}$) Elastic		1st		2nd			3rd		
0^-		$s_{1/2}$		$p_{1/2}$		$d_{3/2}$			$f_{5/2}$		
	−3.624	0.76		−0.75		0.08			0.0		
	5.822	0.01		−0.01		−0.04			0.0		
	9.016	−0.02		−0.09		0.10			0.0		
	10.998	−0.07		−0.02		−0.10			0.0		
	12.689	−0.03		−0.01		0.14			0.0		
	13.251	−0.04		−0.02		1.02			0.0		
	15.029	−0.02		0.00		0.28			0.0		
	15.250	0.02		0.01		−0.18			0.0		
0^+		$p_{1/2}$		$s_{1/2}$		$p_{3/2}$			$d_{5/2}$		
	−17.32	1.23		−0.08		1.26			0.0		
	4.859	−0.02		0.01		−0.12			0.0		
1^-		$s_{1/2}$	$d_{3/2}$	$p_{1/2}$	$p_{3/2}$	$s_{1/2}$	$d_{3/2}$	$d_{5/2}$	$p_{3/2}$	$f_{5/2}$	$f_{7/2}$
	−5.110	0.71	−0.13	0.76	−0.04	0.15	−0.00	−0.23	0.09	0.0	0.0
	−0.345	−0.19	−0.18	−0.14	−0.30	0.71	0.08	−0.05	−0.01	0.0	0.0
	2.939	−0.01	0.73	0.06	−0.02	0.03	0.38	−0.63	0.19	0.0	0.0
	4.741	−0.09	0.12	−0.02	0.00	0.01	0.13	−0.38	0.07	0.0	0.0
	6.264	−0.03	−0.45	−0.01	0.01	−0.05	−0.12	−0.44	−0.01	0.0	0.0
	7.025	0.05	0.30	0.01	−0.01	0.05	0.05	0.39	−0.01	0.0	0.0
	7.927	−0.00	−0.16	−0.05	−0.00	−0.01	−0.06	−0.13	0.00	0.0	0.0
	8.838	0.03	0.03	−0.06	0.00	0.03	0.13	0.06	−0.02	0.0	0.0
	9.753	−0.06	0.12	0.03	0.01	0.01	0.02	−0.17	−0.00	0.0	0.0
	10.832	−0.01	−0.04	−0.01	−0.03	0.01	0.28	0.05	−0.01	0.0	0.0
	11.095	0.04	−0.31	−0.03	0.01	−0.04	0.58	0.07	−0.01	0.0	0.0
	11.662	−0.01	0.08	−0.00	−0.00	0.04	−0.65	−0.26	0.02	0.0	0.0
	12.168	−0.02	−0.05	0.00	−0.01	−0.07	−0.15	−0.09	0.00	0.0	0.0
	13.038	0.00	0.09	−0.00	−0.00	0.01	0.02	−0.10	0.00	0.0	0.0
	13.209	−0.01	0.14	0.01	−0.00	0.03	−0.13	−0.12	0.01	0.0	0.0
	13.996	−0.01	0.03	0.00	0.00	0.02	−0.15	−0.04	0.02	0.0	0.0
	14.639	−0.03	0.00	0.00	0.00	−0.00	−0.24	−0.06	0.02	0.0	0.0
	15.113	−0.00	−0.06	−0.00	−0.00	0.00	0.09	−0.02	−0.01	0.0	0.0
	15.396	−0.00	−0.03	−0.00	0.00	−0.01	0.19	0.01	−0.01	0.0	0.0
	16.049	0.01	0.13	0.01	−0.01	−0.00	−0.20	0.02	0.01	0.0	0.0
1^+		$p_{1/2}$	$p_{3/2}$	$s_{1/2}$	$d_{3/2}$	$p_{1/2}$	$p_{3/2}$	$f_{5/2}$	$d_{3/2}$	$d_{5/2}$	
	1.090	0.01	−0.04	−0.00	0.0	−0.03	0.06	0.0	0.0	0.0	
2^-		$d_{3/2}$	$d_{5/2}$	$p_{3/2}$	$f_{5/2}$	$s_{1/2}$	$d_{3/2}$	$d_{5/2}$	$p_{1/2}$	$p_{3/2}$	$f_{5/2}$	$f_{7/2}$
	−4.733	0.08	1.03	0.13	0.0	0.09	0.04	0.44	−0.80	0.23	0.0	0.0
	0.670	0.17	−0.06	−0.30	0.0	−0.70	−0.06	0.40	−0.01	0.13	0.0	0.0
	2.190	0.89	−0.27	0.07	0.0	0.22	−0.26	0.39	0.07	0.07	0.0	0.0
	4.884	−0.43	−0.25	0.01	0.0	0.14	−0.24	0.55	−0.02	0.12	0.0	0.0
	5.927	−0.38	−0.25	−0.01	0.0	0.09	−0.07	0.45	−0.04	0.10	0.0	0.0
	6.288	−0.00	−0.07	−0.01	0.0	0.02	−0.13	0.12	−0.01	0.04	0.0	0.0
	7.051	−0.12	0.02	−0.01	0.0	−0.03	0.14	0.02	0.02	−0.02	0.0	0.0
	7.586	0.02	−0.06	0.01	0.0	−0.00	−0.01	0.17	−0.01	0.03	0.0	0.0
	8.485	−0.18	0.06	0.02	0.0	−0.01	−0.08	−0.03	0.02	−0.01	0.0	0.0
	8.775	−0.09	0.16	0.01	0.0	−0.04	−0.90	−0.13	0.06	−0.02	0.0	0.0
	8.969	0.11	0.04	0.01	0.0	−0.03	−0.33	−0.37	−0.01	−0.03	0.0	0.0
	10.362	−0.10	−0.03	−0.02	0.0	0.01	0.15	0.16	0.04	0.00	0.0	0.0
	10.744	0.18	−0.08	−0.01	0.0	0.01	0.14	−0.04	−0.01	−0.01	0.0	0.0
	11.249	0.13	−0.05	0.00	0.0	0.03	0.21	0.13	0.01	−0.00	0.0	0.0
	11.832	0.01	−0.04	0.02	0.0	−0.01	0.08	0.07	0.01	0.00	0.0	0.0
	12.395	−0.07	−0.05	−0.00	0.0	0.03	0.10	0.12	0.02	0.00	0.0	0.0

TABLE II. (*Continued*).

J^π	E_λ (MeV)	$\gamma_{\lambda c}$ ($MeV^{1/2}$) Elastic		1st		2nd				3rd			
	12.439	−0.00	−0.01	0.01	0.0	0.01	0.03	0.03		0.00	−0.01	0.0	0.0
	13.270	0.03	−0.02	−0.00	0.0	0.01	0.05	−0.01		0.01	0.01	0.0	0.0
	14.180	−0.11	−0.00	−0.00	0.0	0.01	−0.15	0.02		−0.01	−0.01	0.0	0.0
	14.578	0.05	0.00	−0.00	0.0	−0.01	0.01	0.07		−0.00	0.01	0.0	0.0
	14.727	0.03	−0.00	0.00	0.0	0.01	0.10	0.03		0.01	0.01	0.0	0.0
	15.094	−0.02	−0.03	−0.01	0.0	0.02	0.02	0.04		0.00	0.01	0.0	0.0
	15.198	−0.05	−0.03	0.00	0.0	0.03	−0.04	0.12		0.01	0.01	0.0	0.0
	15.610	0.03	−0.00	−0.01	0.0	0.02	0.01	0.04		0.00	0.00	0.0	0.0
	15.950	−0.05	−0.01	−0.00	0.0	0.01	−0.14	−0.02		−0.01	−0.01	0.0	0.0
	16.062	−0.07	0.01	−0.00	0.0	−0.00	−0.08	0.05		0.00	0.00	0.0	0.0
2^+		$p_{3/2}$	$f_{5/2}$	$d_{3/2}$	$d_{5/2}$	$p_{1/2}$	$p_{3/2}$	$f_{5/2}$	$f_{7/2}$	$s_{1/2}$	$d_{3/2}$	$d_{5/2}$	
	−1.832	−0.16	0.0	0.0	0.0	0.51	−0.27	0.0	0.0	−0.00	0.0	0.0	
	7.223	0.02	0.0	0.0	0.0	−0.04	0.04	0.0	0.0	−0.00	0.0	0.0	
3^-		$d_{5/2}$		$f_{5/2}$	$f_{7/2}$	$d_{3/2}$	$d_{5/2}$			$p_{1/2}$	$p_{3/2}$	$f_{5/2}$	$f_{7/2}$
	−5.206	−1.08		0.0	0.0	0.13	0.09			−0.76	−0.19	0.0	0.0
	0.315	−0.06		0.0	0.0	0.06	−1.12			0.06	0.35	0.0	0.0
	4.128	0.15		0.0	0.0	−0.04	−0.02			−0.02	−0.00	0.0	0.0
	5.209	0.25		0.0	0.0	0.22	0.10			0.01	−0.03	0.0	0.0
	6.419	0.09		0.0	0.0	−0.48	−0.03			−0.10	0.02	0.0	0.0
	7.222	0.03		0.0	0.0	0.04	−0.00			−0.01	−0.02	0.0	0.0
	8.891	0.15		0.0	0.0	0.90	0.04			−0.03	−0.00	0.0	0.0
	9.330	0.03		0.0	0.0	0.07	−0.00			−0.01	−0.03	0.0	0.0
	9.851	−0.00		0.0	0.0	0.07	0.02			0.04	0.00	0.0	0.0
	10.536	0.04		0.0	0.0	0.15	0.05			0.03	0.01	0.0	0.0
	11.555	0.00		0.0	0.0	−0.04	0.01			0.02	0.01	0.0	0.0
	12.109	0.05		0.0	0.0	−0.03	0.00			−0.02	−0.02	0.0	0.0
	12.451	0.01		0.0	0.0	0.02	0.05			0.01	0.01	0.0	0.0
	13.262	0.06		0.0	0.0	0.01	−0.04			−0.01	−0.03	0.0	0.0
	13.658	0.07		0.0	0.0	0.07	0.02			−0.01	0.01	0.0	0.0
	14.015	0.04		0.0	0.0	0.04	−0.06			−0.01	−0.02	0.0	0.0
	14.250	0.01		0.0	0.0	0.03	−0.00			−0.00	0.01	0.0	0.0
	15.134	0.01		0.0	0.0	−0.22	0.09			−0.01	0.01	0.0	0.0
	15.236	0.02		0.0	0.0	−0.06	0.04			−0.01	0.01	0.0	0.0
	15.502	0.02		0.0	0.0	0.02	0.04			0.00	0.01	0.0	0.0

both normal and non-normal parity. This is sometimes referred to as "hard sphere" scattering and has the effect equivalent to scattering from lower-energy or bound states. The B_L, as calculated, are too large because of the interference between the normal parity "hard sphere" scattering and the non-normal parity states. Normal parity states, arising from $2\hbar\omega$ configurations, when included at the upper energies will contribute to the R matrix with the opposite sign from that of the "hard sphere" scattering, and all of the B_L will be reduced in magnitude due to cancellation effects. Preliminary estimates of normal parity states at the upper energies showed this to be true.

The inelastic data were not fitted very well and are not shown. It should be noted that there is no hard sphere scattering for the inelastic channels, so that the previous discussions do not apply here. For both the predictions by Resler[35] and MDR,[36,37] the values are generally too low for the B_0 term and many of the other coefficients were zero, contrary to experiment. Of the three inelastic channels, the calculated B_0 of the second inelastic channel appear closest to the data. The lack of agreement with the other two inelastic channels can again be understood in terms of the absence or near absence of normal parity states in the shell-model calculations. Much of the nonresonant part of the B_0 term is caused by $l=0$ decay. In order to have $l=0$ decay from ^{14}C* states to the first and third excited states of ^{13}C, the ^{14}C* states must be of normal parity. Since normal parity $2\hbar\omega$ states are not present in the model calculations, small B_0 terms result. The second excited state is of opposite parity so it can be formed by $l=0$ decay from the non-normal parity states of ^{14}C* which were calculated.

We noticed that when seven of the lowest-energy states were adjusted in energy (as shown in Fig. 14 by solid connecting lines) so that they matched the experimental energies, the quality of the fits to the data for $E_n < 4$ MeV was significantly increased. However, for $E_n > 4$ MeV, the adjustment of the energy of states to further improve the agreement with the data was not as obvious.

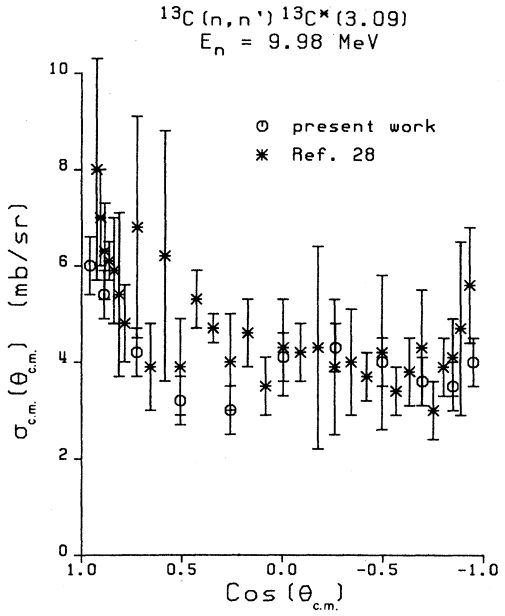

FIG. 9. Comparison of the measurements of the $^{13}C(n,n')^{13}C^*(3.09)$ angular distribution at $E_n = 9.98$ MeV from the present work (○) and from Davè *et al.* (Ref. 28) (*).

B. Fits based on adjustment of the parameters

The latter results of the previous section for $E_n < 4$ MeV were very encouraging. For $E_n > 4$ MeV, it was not this new method which had failed, but the inadequacy of the shell-model calculations themselves by not predicting more completely the normal parity states. Thus, until the model calculations can be extended in this direction, the method of R-matrix fitting by parameter adjustment must be used for the higher energies. A two step approach was employed.

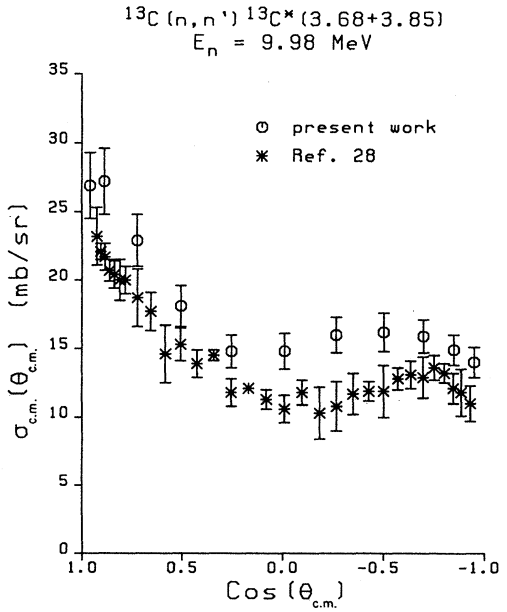

FIG. 10. Comparison of the measurements of the $^{13}C(n,n')^{13}C^*$ (3.68 + 3.85) angular distribution at $E_n = 9.98$ MeV from the present work (○) and from Davè *et al.* (Ref. 28) (*).

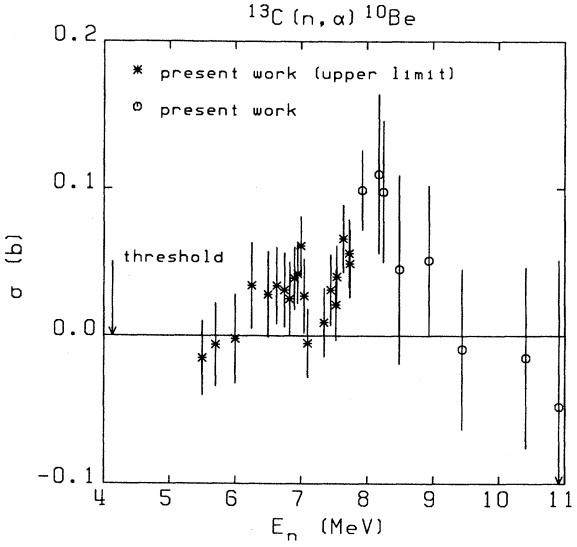

FIG. 11. Estimations of the $^{13}C(n,\alpha)^{10}Be$ integrated cross section from the present work.

1. First step

For the first step, the elastic data of Lane *et al.*[2] were reanalyzed. Starting with Lane's final parameters, the constant R_0 background terms were replaced by broad states above the region of interest in order to simulate more properly the effects of distant states. In addition, some of the parameters for the previous states were modified slightly. Two significant changes were made. The first involved the bound states. As listed in Table I of Lane *et al.*,[2] the level energies E_λ and reduced width amplitudes $\gamma_{\lambda c}$ are not consistent with the excitation energies for the bound 0^- and 1^- states. By replacing the negative R_0's for these J^π's with larger $\gamma_{\lambda c}$'s for those two states the inconsistencies were removed and the corresponding dimensionless reduced widths become $\theta^2(0^-) \approx 0.23$ and $\theta^2(1^-) \approx 0.24$. Lane's results were $\theta^2(0^-) \approx \theta^2(1^-) \approx 0.15$. The agreement with the $^{13}C(d,p)^{14}C$ stripping results of Glover and Jones,[46] $\theta^2(0^-) \approx 0.24$ and $\theta^2(1^-) \approx 0.20$, is now much better. For the second significant change, the sign of the $d_{5/2}$ reduced width amplitude for the 2^- state at $E_x \approx 11.6$ MeV was reversed in order to agree with the shell model calculations. Correspondingly, this forced the $\gamma_{\lambda c}$'s for the 1^+ state at $E_x \approx 11.3$ MeV to be modified as well. The end result was a slightly better overall fit[23] than in the previous work.[2]

Since none of the narrow resonances observed in the total cross section[18] and analyzed in the previous work[2] were reanalyzed here, we refer to the work of Lane *et al.*[2] for a detailed discussion of those narrow states.

TABLE III. Summary of the best adjustment-of-parameters R-matrix fit. The neutron energy is in the laboratory system, the other energies in the center-of-mass system.

E_x (MeV)	E_n (MeV)	E_λ (MeV)	J^π	Γ_T[a] (MeV)
6.09		−4.61	1^-	
6.73		−4.65	3^-	
6.90		−3.22	0^-	
7.34		−4.10	2^-	
11.295	3.358	3.113	1^+	0.17
11.5	3.5	2.4	1^-	2.7
11.6	3.7	3.0	2^-	1.3
12.20	4.33	3.96	1^-	0.37
12.61	4.77	4.40	2^-	0.18
13.7	6.0	5.7	2^-	1.8
14.63	6.95	6.55	(1^-)	0.39
14.717	7.048	6.585	4^+	0.09
14.91	7.26	6.80	(1^+)	0.25
15.56	7.95	7.40	3^-	0.27
15.8	8.3	7.7	(1^-)	0.63
15.91	8.34	7.88	4^+	0.33
16.6	9.1	8.5	(1^+)	0.78
17.7	10.2	9.6	(1^+)	1.3

[a]Estimation from $\sum_c 2P_c\gamma_{\lambda c}^2$.

However, a few comments are necessary on the previous work. From that work, a 3^- state and a 1^- state were located at $E_x=9.789$ MeV ($E_n=1.737$ MeV) and $E_x=9.806$ MeV ($E_n=1.755$ MeV), respectively. This 1^- state interferes with the large 1^- background and produces the dip observed in the B_0 term of the elastic (or total in this case) cross section around $E_n\approx 1.7$ MeV.[2,18] While clearly observed in the work of Lane *et al.*,[2] this state was omitted from the latest compilation.[47] As further proof of this state's existence, the shell-model calculations of Resler[35] and MDR (Refs. 36 and 37) show a 1^- state in this region, and when the energy of the state is adjusted slightly to the energy claimed by Lane, a dip is produced in the elastic (total) cross section as observed experimentally. The total cross section and the elastic scattering data show a large resonance structure around $E_n\approx 3.5$ MeV. The work of Lane *et al.*[2] indicated that four major states made up this structure: a very broad 1^- state, a very broad 2^- state, a somewhat narrower 1^- state, and a 1^+ state. None of the negative parity states were included in the latest compilation.[47] Shell-model calculations of Resler[35] and of MDR (Refs. 36 and 37) predicted these very broad 1^- and 2^- states with the resulting spectroscopic amplitudes being consistent with the R-matrix analysis of Lane *et al.*[2]—except for the sign of one reduced width amplitude for the 2^- state.

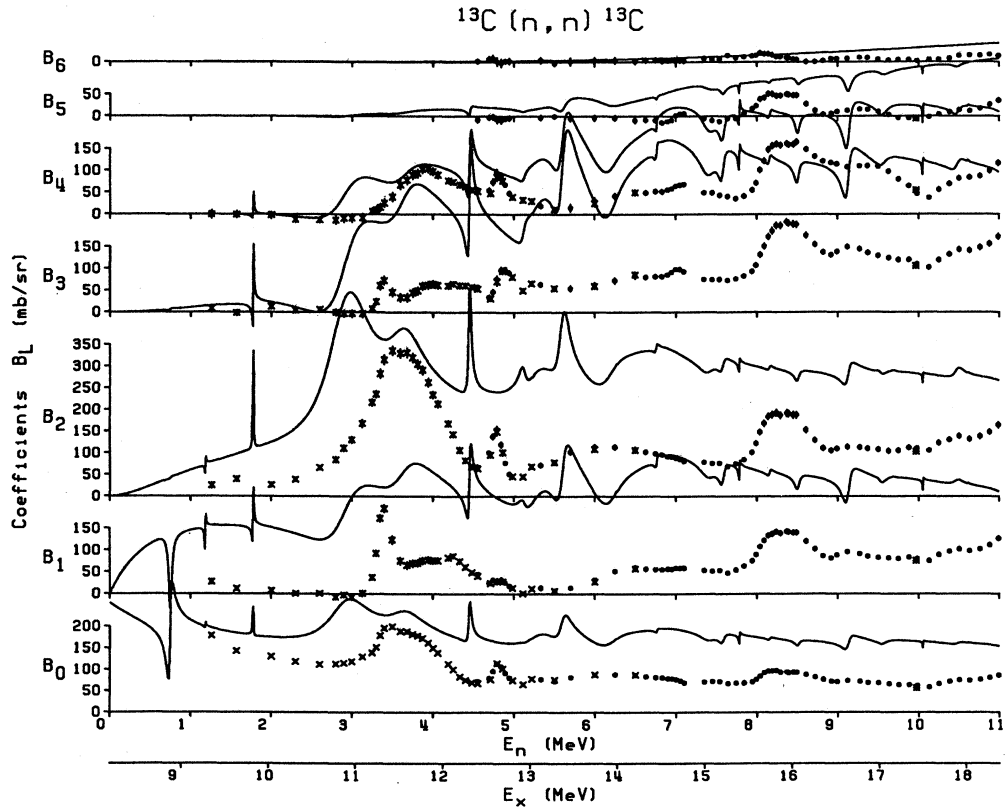

FIG. 12. Comparison of the R-matrix fit predicted by Resler's (Ref. 35) shell-model results to the elastic data of Lane *et al.* (Ref. 2) (×) ($0\le E_n\le 6.5$ MeV), of the present work (●) ($4.55\le E_n\le 11$ MeV), and of Davè *et al.* (Ref. 28) (*) ($E_n=10$ MeV).

TABLE IV. Full parameter set used in the best adjustment-of-parameters R-matrix fit.

J^π	E_λ (MeV)	$\gamma_{\lambda c}$ ($MeV^{1/2}$) Elastic		1st		2nd				3rd			
0^-		$s_{1/2}$		$p_{1/2}$		$d_{3/2}$				$f_{5/2}$			
	−3.225	0.88		−0.75		0.08				0.0			
0^+		$p_{1/2}$		$s_{1/2}$		$p_{3/2}$				$d_{5/2}$			
	14.4	1.95		1.80		0.0				0.0			
1^-		$s_{1/2}$	$d_{3/2}$	$p_{1/2}$	$p_{3/2}$	$s_{1/2}$	$d_{3/2}$	$d_{5/2}$		$p_{3/2}$	$f_{5/2}$	$f_{7/2}$	
	−4.615	0.90	−0.13	0.76	−0.04	0.15	0.0	−0.23		0.09	0.0	0.0	
	2.383	0.398	1.384	0.0	0.0	0.03	0.38	−0.63		0.19	0.0	0.0	
	3.957	0.295	0.167	0.0	0.0	0.01	0.13	−0.38		0.07	0.0	0.0	
	6.55	0.17	0.0	−0.1	0.0	0.0	0.0	−0.5		0.0	0.0	0.0	
	7.69	0.20	0.35	0.08	−0.02	0.0	0.0	0.0		0.0	0.0	0.0	
	10.63	−0.043	2.224	0.0	0.0	−0.80	0.0	0.0		0.0	0.0	0.0	
1^+		$p_{1/2}$	$p_{3/2}$	$s_{1/2}$	$d_{3/2}$	$p_{1/2}$	$p_{3/2}$	$f_{5/2}$		$d_{3/2}$	$d_{5/2}$		
	3.113	0.219	−0.139	0.0	0.0	0.0	0.0	0.0		0.0	0.0		
	6.8	0.10	0.0	0.0	−0.4	0.0	0.0	0.0		0.0	0.0		
	8.5	0.2	0.2	0.1	0.1	0.2	0.2	0.0		−0.1	0.1		
	9.65	0.25	0.25	0.01	−0.3	−0.2	−0.2	0.0		−0.1	0.2		
	15.478	−0.132	2.142	0.5	0.0	0.0	0.0	0.0		0.0	0.0		
	15.583	1.796	0.103	0.5	0.0	0.0	0.0	0.0		0.0	0.0		
2^-		$d_{3/2}$	$d_{5/2}$	$p_{3/2}$	$f_{5/2}$	$s_{1/2}$	$d_{3/2}$	$d_{5/2}$		$p_{1/2}$	$p_{3/2}$	$f_{5/2}$	$f_{7/2}$
	−4.096	0.08	1.03	0.13	0.0	0.09	0.04	0.44		−0.80	0.23	0.0	0.0
	3.016	0.981	−0.286	−0.30	0.0	0.22	−0.26	0.39		0.07	0.07	0.0	0.0
	4.40	0.30	0.10	0.0	0.4	0.0	0.0	0.0		0.0	0.0	0.0	0.0
	5.72	0.80	0.0	0.0	−0.2	−0.15	0.8	0.05		0.0	0.0	0.0	0.0
	13.9	1.9	0.0	0.0	0.0	1.1	0.0	0.0		0.0	0.0	0.0	0.0
2^+		$p_{3/2}$	$f_{5/2}$	$d_{3/2}$	$d_{5/2}$	$p_{1/2}$	$p_{3/2}$	$f_{5/2}$	$f_{7/2}$	$s_{1/2}$	$d_{3/2}$	$d_{5/2}$	
	14.9	2.5	0.0	0.0	0.0	0.0	0.0	0.0	0.0	1.0	0.0	0.0	
	15.1	0.0	1.7	0.0	0.0	0.0	0.0	0.0	0.0	0.0	0.0	0.0	
3^-		$d_{5/2}$		$f_{5/2}$	$f_{7/2}$	$d_{3/2}$	$d_{5/2}$			$p_{1/2}$	$p_{3/2}$	$f_{5/2}$	$f_{7/2}$
	−4.654	−1.08		0.0	0.0	0.13	0.09			−0.76	−0.19	0.0	0.0
	7.40	0.25		0.0	0.0	0.0	0.0			0.15	−0.06	0.0	0.0
	15.1	1.28		0.0	0.0	0.0	0.0			0.0	0.0	0.0	0.0
3^+		$f_{5/2}$	$f_{7/2}$	$d_{5/2}$		$p_{3/2}$	$f_{5/2}$	$f_{7/2}$		$s_{1/2}$	$d_{3/2}$	$d_{5/2}$	
	15.6	0.8	0.0	0.0		0.0	0.0	0.0		0.0	0.0	0.0	
4^+		$f_{7/2}$				$f_{5/2}$	$f_{7/2}$			$d_{3/2}$	$d_{5/2}$		
	6.585	0.110				0.0	0.0			0.198	0.242		
	7.878	0.220				0.0	0.0			0.18	0.38		

The present work shows that the data can be equally well fitted by changing this sign and the sign for one of the 1^+ reduced width amplitudes.

2. *Second step*

The set of R-matrix parameters discussed above was used as the starting point for an adjustment-of-parameters fitting of the entire elastic and inelastic data set for $E_n \leq 11$ MeV. Inelastic widths were added to most of these states as given by shell-model calculations of Resler.[35] Next, inelastic widths were added to the distant broad states as necessary to produce the nonresonant structure observed in the B_0 terms of the three inelastic channels. Once that was accomplished, various numbers of states of various J^π's and various $\gamma_{\lambda c}$'s were tried in various locations for $4.5 \leq E_n \leq 11$ MeV in an attempt to fit the new data. Several thousand parameter variations were attempted, and shown in Figs. 5, 6, 7, and 8 are the best fits to the data which were obtained. A summary of the resulting J^π values and excitation energies is shown in Table III. The full parameter set is shown in Table IV. Specifics on the new states will now be given. A full dis-

cussion is given in Ref. 23.

In the elastic-only work of Lane *et al.*,[2] the state of $E_x = 12.61$ MeV ($E_n = 4.77$ MeV) was assigned tentatively as 2^- or 3^- with 3^- giving a slightly better fit. In the present work, many parameter variations were tried; however, it was determined that a 3^- assignment could not produce the structure seen in the coefficients of the first inelastic cross section. Only the 2^- assignment fit the data reasonably well. In addition, the very broad structure centered around $E_n \approx 6$ MeV was best fitted by a broad 2^- state. In the previous elastic-only work by Lane *et al.*[2] this state was tentatively assigned 1^- or 2^-.

Three states were located near $E_n \approx 7$ MeV ($E_x \approx 14.7$ MeV). An inspection of the total cross section shows small resonances in this region. While little structure is observed in the elastic cross section, the three inelastic channels show evidence of several states. The most unique feature is the very narrow resonance observed in the third inelastic channel at $E_n = 7.05$ MeV. After many trial fits, only a 4^+ state could produce the observed structure. Both B_0 and B_4 are fitted well. The interference terms B_1 and B_3 appear with the wrong sign—most likely indicating an incorrect sign on some of the $\gamma_{\lambda c}$'s of the high-energy broad states. The wider structure in the B_2 term which is not fitted is probably caused by another state slightly lower in energy. Our best fit also includes two other states near $E_n \approx 7$ MeV, a 1^- state at $E_n = 6.95$ ($E_x = 14.91$ MeV). While these two states reproduce some of the observed structure, other structures are not reproduced. Hence, these two assignments are tentative.

The next three states of the present fit are located in the region $8 < E_n < 9$ MeV. Both the total cross section and the elastic cross section show very pronounced broad resonance structure in this region. Again, the most unique feature occurs in the third inelastic channel. Except for the B_2 term, all of the other B_L terms were fitted with a 4^+ state at $E_n = 8.34$ MeV ($E_x = 15.91$ MeV). A 3^- state slightly lower in energy at $E_n = 7.95$ MeV ($E_x = 15.56$ MeV) was the only state which would, along with the 4^+ state, reproduce the remaining structure observed in the B_0, B_1, and B_2 terms of the third inelastic channel. This 3^- state also appears to be largely responsible for the structure observed in the elastic cross section. Also in this region, a tentative 1^- state at $E_n = 8.3$ MeV ($E_x = 15.8$ MeV) reproduces the peak observed in the B_1 term of the first inelastic channel. As with the previous group of states, there is a large probability that additional states are required in this region. The latest compilation[47] shows many states (mostly without J^π assignments) for $E_x > 15$ MeV; however, none appear to correspond in energy to these three states from the present work.

Two 1^+ states based on the latest compilation[47] were included for the region $E_n > 9$ MeV. The remaining

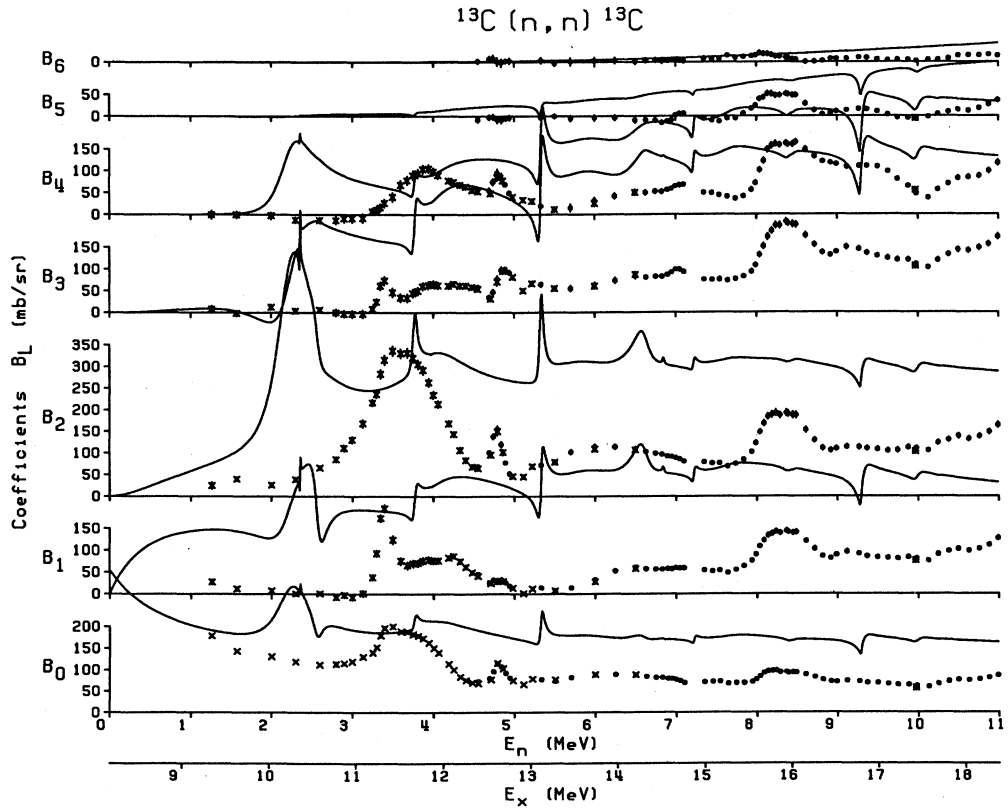

FIG. 13. Comparison of the R-matrix fit predicted by the MDR (Refs. 36 and 37) shell-model results to the elastic data of Lane *et al.* (Ref. 2) ($\times$) ($0 \leq E_n \leq 6.5$ MeV), of the present work (●) ($4.55 \leq E_n \leq 11$ MeV), and of Davè *et al.* (Ref. 28) (*) ($E_n = 10$ MeV).

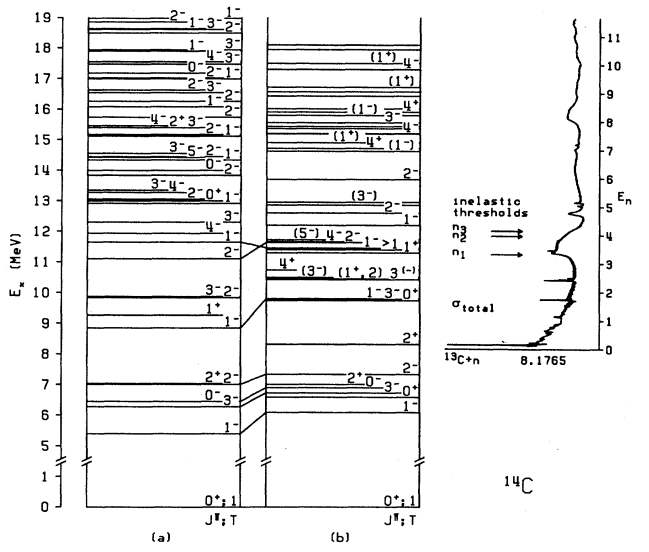

FIG. 14. The ^{14}C shell-model results of Resler (Ref. 35) are shown in energy level diagram (a) and the proposed level scheme of ^{14}C based on experiment (see Table V) is shown in energy level diagram (b). Shown on the right is the $^{13}C+n$ total cross section from Cohn *et al.* (Ref. 17) ($E_n < 1.2$ MeV) and Auchampaugh *et al.* (Ref. 18) ($E_n > 1.2$ MeV).

states at higher energies are very broad and were included to simulate the effects of distant states. Widths for these states were largely determined from the elastic only fitting. These levels should not be considered as actual states in ^{14}C, but should only be used to determine the overall strengths from states at higher energies.

No detailed comparisons of the present results for ^{14}C were made to other $A=14$ results since there are no levels in ^{14}O of known spin or parity above $E_x=10$ MeV [$E_x(^{14}C)\approx 10$ MeV] (Ref. 47) for comparison, and since for ^{14}N almost all of the known levels above $E_x(^{14}N)=16$ MeV [$E_x(^{14}C)\approx 14$ MeV] are of mixed isospin,[47] thus making comparisons uncertain. The results of the shell-model calculations and R-matrix analyses of the present work were combined with information from the literature in order to determine the best current knowledge of the level structure of ^{14}C. Shown in Table V and Fig. 14 are the proposed energy levels of ^{14}C obtained by merging all the available information.

IV. CONCLUSIONS

Using the time-of-flight facilities of the Ohio University Accelerator Laboratory, differential cross sections for neutrons elastically scattered from ^{13}C and inelastically scattered to the first three excited states $^{13}C^*$ (3.09, 3.68, and 3.85 MeV) were measured at 69 incident neutron energies (9 to 11 angles per energy) from $E_n=4.5$ MeV to $E_n=10.99$ MeV. In all, 2742 differential cross sections for $^{13}C+n$ were measured. Where these data overlapped with existing data, excellent agreement was obtained.

A new multiple scattering code MACHO was developed for this work.[24] By providing a very detailed simulation of the entire experimental scattering process, accurate corrections to the small inelastic cross sections were obtained. In addition to multiple scattering, corrections were obtained that (1) removed the elastic scattering of the neutron source continuum from under the small inelastic cross sections, (2) removed the effects of the 2.2-atom-percent hydrogen impurity, and (3) resolved the in-

TABLE V. Proposed energy levels of ^{14}C. Proof for the indicated levels are from the latest compilation (Ref. 47) (C), Lane *et al.* (Ref. 2) (L), and the present work (R).

E_x (MeV)	$J^\pi;T$	Γ (keV)	Proof
0.0	$0^+;1$		C
6.094	1^-		C
6.589	0^+		C
6.728	3^-		C
6.903	0^-		C
7.012	2^+		C
7.341	2^-		C
8.318	2^+	3.4	C
9.746	0^+		C
9.789	3^-	15	L
9.806	1^-	41	L,R
10.429	$3^{(-)}$	10	L
10.447	$(1^+,2^\pm)$	7	L
10.498	(3^-)	$\ll 5$	C,L
10.736	4^+	20	C
11.295	1^+	170	C,L,R
11.395	≥ 2	<7	L
11.46	1^-	2800	L,R
11.64	2^-	1300	L,R
11.666	4^-	20	C
11.730	(5^-)		C
12.20	1^-	370	L,R
12.61	2^-	180	R
12.863		30	C
12.963	(3^-)	30	C
13.7	2^-	1800	R
14.63	(1^-)	390	R
14.717	4^+	90	R
14.91	(1^+)	250	R
15.20	4^-		C
(15.37)			C
15.44			C
15.56	3^-	270	R
15.8	(1^-)	630	R
15.91	4^+	330	R
(16.02)			C
16.43			C
(16.57)			C
16.715	(1^+)	≈ 200	C
17.30	4^-		C
(17.5)	(1^+)	≈ 200	C
17.95			C
18.10			C
20.4		wide	C
22.1			C
24.3	$4^-;2$	<300	C
24.5		wide	C

elastic scattering cross sections to the second and third excited states over the entire range of energies. An estimation of the integrated $^{13}C(n,\alpha)^{10}Be$ cross section was obtained up to $E_n = 11$ MeV.

Shell-model calculations from Resler[35] and MDR (Refs. 36 and 37) were used to generate the R-matrix parameters for the elastic and first three inelastic channels of $^{13}C+n$. After the slight adjustment of some energies, the predicted cross sections generally agreed with experiment for $E_n < 4$ MeV. However, calculations of the normal parity states of $2\hbar\omega$ and higher are required in order to predict more correctly cross sections above $E_n \approx 4$ MeV.

The elastic $^{13}C+n$ data of Lane *et al.*[2] were refitted in order to replace the R_0 background terms by more realistic broad states, to obtain better agreement with the signs of the shell-model spectroscopic amplitudes, and to obtain a better fit to the data. The adjustment-of-parameters R-matrix fitting of the full $^{13}C+n$ data set has produced new level information on ^{14}C. For $E_n > 4.5$ MeV ($E_x > 12.5$ MeV), five states were given definite J^π assignments and three states were given tentative assignments. The new information on ^{14}C obtained from this work has been merged with the existing information to arrive at the level structure of ^{14}C presented here.

ACKNOWLEDGMENTS

The authors would like to express their appreciation to M. Cates and J. Fréhaut for providing us with their unpublished $(n,2n)$ data and to D. J. Millener and F. Darema-Rogers for providing us with their unpublished ^{14}C shell model calculations. Comments by F. C. Barker on the transformation of shell model to R-matrix quantities were greatly appreciated. We warmly thank Dave Sturbois and Don Carter of the accelerator staff for their many hours of hard work which were required for the completion of the experimental work. We also thank John O'Donnell for his help with computer related aspects of this work. This work was supported by the U.S. Department of Energy.

*Present address: Lawrence Livermore National Laboratory, Livermore, CA 94550.

†Present address: Los Alamos National Laboratory, Los Alamos, NM 87545.

[1]F. Ajzenberg-Selove, Nucl. Phys. **A360**, 1 (1981).

[2]R. O. Lane, H. D. Knox, P. Hoffmann-Pinther, R. M. White, and G. F. Auchampaugh, Phys. Rev. C **23**, 1883 (1981).

[3]F. Ajzenberg-Selove, H. G. Bingham, and J. D. Garrett, Nucl. Phys. **A202**, 152 (1973).

[4]F. Ajzenberg-Selove, E. R. Flynn, and Ole Hansen, Phys. Rev. C **17**, 1283 (1978).

[5]S. Mordechai, H. T. Fortune, G. E. Moore, M. E. Cobern, R. V. Kollarits, and R. Middleton, Nucl. Phys. **A301**, 463 (1978).

[6]J. N. McGruer, E. K. Warburton, and R. S. Bender, Phys. Rev. **100**, 235 (1955).

[7]R. L. McGrath, Phys. Rev. **145**, 802 (1966).

[8]R. Jahn, G. J. Wozniak, D. P. Stahel, and J. Cerny, Phys. Rev. Lett. **37**, 812 (1976).

[9]R. Jahn, D. P. Stahel, G. J. Wozniak, R. J. de Meijer, and J. Cerny, Phys. Rev. C **18**, 9 (1978).

[10]J. van Driel, R. Kamermans, and R. J. de Meijer, Nucl. Phys. **A350**, 109 (1980).

[11]M. Hamm and K. Nagatani, Phys. Rev. C **17**, 586 (1978).

[12]S. Dahlgren, P. Grafström, B. Höistad, and A. Åsberg, Phys. Lett. **47B**, 439 (1973).

[13]D. B. Holtkamp, S. J. Seestrom-Morris, S. Chakravarti, D. Dehnhard, H. W. Baer, C. L. Morris, S. J. Greene, and C. J. Harvey, Phys. Rev. Lett. **47**, 216 (1981).

[14]H. Crannell, J. M. Finn, P. Hallowell, J. T. O'Brien, N. Ensslin, L. W. Fagg, E. C. Jones, Jr., and W. L. Bendel, Nucl. Phys. **A278**, 253 (1977).

[15]H. W. Baer, J. A. Bistirlich, N. de Botton, S. Cooper, K. M. Crowe, P. Truöl, and J. D. Vergados, Phys. Rev. C **12**, 921 (1975).

[16]G. Kaschl, G. Mairle, H. Mackh, D. Hartwig, and U. Schwinn, Nucl. Phys. **A178**, 275 (1971).

[17]H. O. Cohn, J. K. Bair, and H. B. Willard, Phys. Rev. **122**, 534 (1961).

[18]G. F. Auchampaugh, S. Plattard, and N. W. Hill, Nucl. Sci. Eng. **69**, 30 (1979).

[19]P. E. Koehler, D. A. Resler, H. D. Knox, R. M. White, and R. O. Lane, Bull. Am. Phys. Soc. **24**, 656 (1979).

[20]D. A. Resler, P. E. Koehler, H. D. Knox, and R. O. Lane, Bull. Am. Phys. Soc. **27**, 628 (1982).

[21]D. A. Resler, P. E. Koehler, H. D. Knox, G. Randers-Pehrson, and R. O. Lane, Bull. Am. Phys. Soc. **27**, 716 (1982).

[22]R. W. Finlay, C. E. Brient, D. E. Carter, A. Marcinkowski, S. Mellema, G. Randers-Pehrson, and J. Rapaport, Nucl. Instrum. Methods **198**, 197 (1982).

[23]D. A. Resler, Ohio University Report No. DOE-ER-02490-5, Ph.D. thesis, 1987.

[24]D. A. Resler and E. T. Sadowski, Nucl. Instrum. Methods **A269**, 607 (1988).

[25]P. E. Koehler, H. D. Knox, D. A. Resler, R. O. Lane, and D. J. Millener, Nucl. Phys. **A394**, 221 (1983).

[26]H. D. Knox, D. A. Resler, and R. O. Lane, Nucl. Phys. **A466**, 245 (1987).

[27]P. E. Koehler, H. D. Knox, D. A. Resler, R. O. Lane, and G. F. Auchampaugh, Nucl. Phys. **A453**, 429 (1986).

[28]J. H. Davè, C. R. Gould, L. W. Seagondollar, C. R. Howell, R. S. Pedroni, F. O. Purser, and R. L. Walter, Nucl. Sci. Eng. **80**, 388 (1982).

[29]J. S. Petler, M. S. Islam, R. W. Finlay, and F. S. Dietrich, Phys. Rev. C **32**, 673 (1985).

[30]G. C. Wick, Phys. Rev. **75**, 1459 (1949).

[31]D. A. Resler, R. O. Lane, and H. D. Knox, Phys. Rev. C **35**, 855 (1987).

[32]M. R. Cates, private communication.

[33]J. Fréhaut, M. Cates, and G. Mosinski, in Centre d'Etudes de Bruyères-le-Châtel Report NEANDC(E) No. 194"L", edited by A. Michaudon, D. Didier, and M. Soleilhac, 1978 (unpublished), p. 66.

[34]A. M. Lane and R. G. Thomas, Rev. Mod. Phys. **30**, 257 (1958).

[35]D. A. Resler, Ohio University Report No. DOE-ER-40387-3, 1989.

[36]D. J Millener and F. Darema-Rogers, private communication.
[37]D. J. Millener, private communication.
[38]S. Cohen and D. Kurath, Nucl. Phys. **73**, 1 (1965).
[39]D. J. Millener and D. Kurath, Nucl. Phys. **A255**, 315 (1975).
[40]A. M. Lane, Rev. Mod. Phys. **32**, 519 (1960).
[41]F. C. Barker, private communication.
[42]F. C. Barker, private communication.
[43]F. C. Barker, Aust. J. Phys. **25**, 341 (1972).
[44]F. C. Barker, Aust. J. Phys. **24**, 777 (1971).
[45]F. C. Barker, H. J. Hay, and P. B. Treacy, Aust. J. Phys. **21**, 239 (1968).
[46]R. N. Glover and A. D. W. Jones, Nucl. Phys. **A84**, 673 (1966).
[47]F. Ajzenberg-Selove, Nucl. Phys. **A449**, 1 (1986).